

ACCEPTED MANUSCRIPT

Multi-legged steering and slipping with low DoF hexapod robots

To cite this article before publication: Dan Zhao *et al* 2020 *Bioinspir. Biomim.* in press <https://doi.org/10.1088/1748-3190/ab84c0>

Manuscript version: Accepted Manuscript

Accepted Manuscript is “the version of the article accepted for publication including all changes made as a result of the peer review process, and which may also include the addition to the article by IOP Publishing of a header, an article ID, a cover sheet and/or an ‘Accepted Manuscript’ watermark, but excluding any other editing, typesetting or other changes made by IOP Publishing and/or its licensors”

This Accepted Manuscript is © 2020 IOP Publishing Ltd.

During the embargo period (the 12 month period from the publication of the Version of Record of this article), the Accepted Manuscript is fully protected by copyright and cannot be reused or reposted elsewhere.

As the Version of Record of this article is going to be / has been published on a subscription basis, this Accepted Manuscript is available for reuse under a CC BY-NC-ND 3.0 licence after the 12 month embargo period.

After the embargo period, everyone is permitted to use copy and redistribute this article for non-commercial purposes only, provided that they adhere to all the terms of the licence <https://creativecommons.org/licenses/by-nc-nd/3.0>

Although reasonable endeavours have been taken to obtain all necessary permissions from third parties to include their copyrighted content within this article, their full citation and copyright line may not be present in this Accepted Manuscript version. Before using any content from this article, please refer to the Version of Record on IOPscience once published for full citation and copyright details, as permissions will likely be required. All third party content is fully copyright protected, unless specifically stated otherwise in the figure caption in the Version of Record.

View the [article online](#) for updates and enhancements.

Multi-legged Steering and Slipping with Low DoF Hexapod Robots

Dan Zhao

Graduate Research Assistant
 Department of Mechanical Engineering
 University of Michigan
 Ann Arbor, Michigan 48105
 Email: danzhaoy@umich.edu

Shai Revzen

Associate Professor
 Department of Electrical Engineering and Computer Science
 University of Michigan
 Ann Arbor, Michigan 48105
 Email: shrevzen@umich.edu

CONTENTS

1	Introduction	
2	1.1 Previous work on multi-legged robots	1
3	1.2 Maneuverability in biological hexapods	2
4	1.3 Definition of steering with a periodic gait	2
5	1.4 Phase constraints limit periodic gaits	2
6	1.5 The geometry of steering strategies	4
7	1.5.1 Changing timing to steer	4
8	1.5.2 The special case of bilateral symmetry in the plane	4
9	1.6 Performance criteria for steering	5
10		
11	2 Multi-legged steering with low DoF legs	5
12	2.1 Steering with these conditions is hard	5
13	2.2 1-DoF steering creates conflicting constraints	6
14		
15	3 Results: low-DoF hexapods steer with slipping	6
16	3.1 BigAnt 1-DoF hexapedal robot	6
17	3.1.1 BigAnt steering gaits	7
18	3.1.2 BigAnt steering gait test results	7
19	3.1.3 BigAnt turning rate results and slipping results	8
20	3.2 Mechapod 2-DoF hexapedal robot	9
21	3.2.1 Mechapod non-slip steering gaits	9
22	3.2.2 Mechapod steering gaits with slipping	11
23		
24	4 Conclusion and discussion	17
25	5 Future work	17

Abstract

Thanks to their sprawled posture and multi-legged support, stability is not as hard to achieve for hexapodal robots as it is for bipeds and quadrupeds. A key engineering challenge with hexapods has been to produce insect-like agility and maneuverability, of which steering is an essential part. However, the mechanisms of multi-legged steering are not always clear, especially for robots with underactuated legs. Here we propose a formal definition of steering, and show why steering is difficult for robots with 6 or more underactuated legs. We show that for many of these robots, steering is impossible without slipping, and present experimental results which demonstrate the importance of allowing for slipping to occur intentionally when optimizing steering ability. Our results suggest that a non-holonomic multi-legged slipping model might be more appropriate than dynamic models for representing such robots, and that conventional non-slip contact models might miss significant parts of the performance envelope.

1 Introduction

Most animals and mobile robots move through the world by moving parts of their body to generate reaction forces from the environment and thereby propel themselves. Legged locomotion focuses on that subset of locomotion that employs intermittent contact forces generated by dedicated organs, the “legs”, for that propulsion. This is distinct from using fluid dynamic forces, as in fish swimming, or continuous contact forces, as in wheeled vehicles. There are very few non-novelty commercial legged robots, and much of the focus in the field of legged robotics has been on bipedal or

1 quarupedal robots. This is stark contrast to the natural world,
 2 where almost all animal groups that employ legs, employ six
 3 or more legs. Much of the objection to building robots with
 4 many legs has been the mechanical complexity of the associated
 5 device, which is directly tied to the number of Degrees
 6 of Freedom (DoF) in each legs (both actuated and unactuated).
 7

8 In this paper we explore steering and slipping in hexape-
 9 dal robots with legs with 1 or 2 DoF, i.e. legs whose point(s)
 10 of contact can only occupy a 1- or 2-dimensional manifold
 11 with respect to the body frame of reference. We draw atten-
 12 tion to the importance and inherent difficulty of producing
 13 steering from such legs. We offer two contributions: (1) ex-
 14 perimental results showing that slipping is highly beneficial
 15 for obtaining an increased steering range, suggesting that the
 16 practice of designing non-slip gaits misses an important part
 17 of the operational envelope of multi-legged robots; (2) evi-
 18 dence that despite slipping, in our hexapods the relationship
 19 between body frame motion and shape change appears to be
 20 “geometric”, i.e. computable knowing only shape and the
 21 rate of shape change, without knowing forces.

22 Below we provide some background (1.1), biological
 23 motivation (1.2), followed by theoretical preliminaries that
 24 precisely define the notion of steering as we use the term
 25 (1.3). We then discuss some of the impact of phase con-
 26 straints on steering gaits (1.4), discuss steering strategies
 27 (1.5), and define the performance metrics we use to eval-
 28 uate steering (1.6).

30 1.1 Previous work on multi-legged robots

31 The conventional approach to studying steering behav-
 32 ior in robots is to directly test proposed steering gaits on
 33 robot platforms and further explore the experimental results
 34 to explain and improve the achieved gaits. For fully actu-
 35 ated hexapod robots (active DoF per leg $d \geq 3$) inverse kine-
 36 matics has been used to plan footholds for precise quasi-
 37 static steering [Duan et al., 2009; Roy and Pratihar, 2014].
 38 However, multi-legged robots do not require fully articu-
 39 lated legs for dynamic stability. Even with 1 DoF or 2 DoF
 40 legs, hexapedal robots can still achieve stability and maneu-
 41 verability — for example the RHex robot family [Galloway
 42 et al., 2010; Saranli et al., 2001] and the Sprawl robot family
 43 [Kim et al., 2006; McClung, 2006]. With all the actuators
 44 concentrated in the body, such low-DoF hexapod robots have
 45 lighter legs which can swing much faster than fully articu-
 46 lated legs, and further boost the speed of locomotion. They
 47 are also simpler to build and less complex to control com-
 48 pared with their fully articulated counterparts.

49 Several investigators have looked at maneuverability of
 50 hexapods: McClung [2006] did a thorough investigation of
 51 the dynamic maneuverability of Sprawlettes (2 DoF per leg)
 52 and identified effective parameters that can be used for steer-
 53 ing. Many interesting turning methods were also tested and
 54 studied on the RoACH family of rapidly-prototyped palm-
 55 size robots [Haldane and Fearing, 2014; Pullin et al., 2012;
 56 Zarrouk and Fearing, 2015]. For OctoRoACH, Pullin
 57 et al. [2012] applied a differential speed method for dy-

1 namic turning by driving legs on different sides with a
 2 different frequency. Haldane and Fearing [2014] demon-
 3 strate that oscillations in height and roll angle determine Ve-
 4 lociRoACH’s turning behavior and developed a steering gait
 5 for VelociRoACH controlled by phase offset between the left
 6 and right sets of legs. 1STAR in [Zarrouk and Fearing, 2015]
 7 claimed to be the first steerable robot with only one actuator;
 8 it generated rotation by continuously accelerating and decel-
 9 erating the legs resulting in the compliance disparity between
 10 alternate stance tripods. Zarrouk et al. [2015] also summa-
 11 rized the turning performance of these three palm-size robots
 12 and other famous multi-legged robots.

13 1.2 Maneuverability in biological hexapods

14 Unlike bipedal and most quadrupedal vertebrates, in-
 15 sects have legs sprawled outward in fore-aft and lateral di-
 16 rections, which offers them additional stability and excep-
 17 tional maneuverability in horizontal plane, making them able
 18 to execute very tight turns at high speeds [McClung, 2006].
 19 Even with similar sprawled structure, achieving such maneu-
 20 verability in hexapedal robots is challenging. Getting better
 21 understanding of the steering behaviors is an essential part of
 22 improving planar maneuverability.

23 One approach is to study animal turning behavior and
 24 build models and hypothesis that would inspire robot design.
 25 Franklin et al. [1981] discovered two principal methods the
 26 cockroach *Blattella germanica* used to turn: increasing step
 27 frequency or step length of legs on one side of the body rela-
 28 tive to the other, where the step length change was achieved
 29 by changing either the leg arc swing magnitude or functional
 30 length of the legs. Some extreme changes of step length like
 31 pivoting one leg in place or even moving one leg backwards
 32 were observed in bee turning by Zolotov et al. [1975]. Jin-
 33 drich and Full [1999] measured the full dynamics of turning
 34 in the cockroach *Blaberus discoidalis* and analyzed the
 35 contributions of each leg to turning, concluding that turning
 36 dynamics can be characterized as a minor modification of
 37 straight-ahead running. To describe motion of cockroaches
 38 in the horizontal plane, several models were developed by
 39 Proctor and Holmes [2008]; Schmitt and Holmes [2000];
 40 Seipel et al. [2004]. Our own study of running *Blaberus dis-
 41 coidalis* cockroaches [Sachdeva et al., 2018] observed that
 42 a large fraction of cockroach foot motions are “slipping” in
 43 the sense that the feet are moving with respect to the ground
 44 while in contact with it as shown in fig. 1. It seems that the
 45 cockroaches exhibit far less non-slip ground contact than as-
 46 sumed in published locomotion models.

47 1.3 Definition of steering with a periodic gait

48 Legged systems (animals and robots both) typically
 49 move using a *periodic gait*¹: a cyclic shape-change which
 50 produces (at least on average) a motion through the world.
 51 The shape-change can be represented by the leg motions in
 52 the body frame of the system. Thus, each leg is repeating the

53 ¹ Some authors conflate the term “gait” with “periodic gait”; the def-
 54 inition and discussion of non-periodic gaits is outside the scope of this
 55 manuscript.

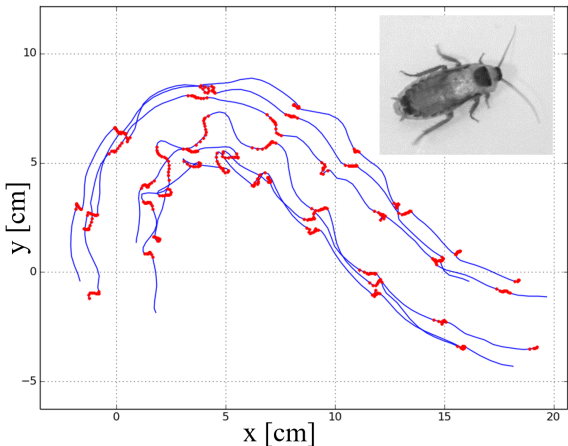


Fig. 1: Cockroaches slip while running. We recorded 24 trials of *Blaberus discoidalis* running at 15–77 cm/s on foam-core [Elmer’s 900803 Foam Board]. On average, front, middle, and hind legs slipped 21%, 18%, 20% of their total travel distance. We show the tarsus (foot) trajectories recorded in the world frame while moving forward relative to the body (blue), and while moving backward (red). Note: synchronized side-view videos suggest that feet moving back with respect to the body are in contact with the ground.

same motions every period of a periodic gait, and the body is thereby propelled in a similar way each cycle.

For moving on a horizontal plane, we typically desire robots to allow us to control position and heading. We will refer (by slight abuse of terminology) to the rigid body motion generated (at least on average) by a single period of a periodic gait as the *holonomy* of that gait. The framework of geometric mechanics provides a precise language for describing how holonomies arise from periodic shape changes [Bloch et al., 2005; Marsden and Ostryowski, 1998]. The partitioning of configuration into body frame and (body) shape is so intuitive that most of the time we assume its validity without careful examination, however, as a technical point, we note that geometric mechanics shows that when the mechanics of a system are governed by a Lagrangian symmetric under the Lie group $SE(2)$, i.e. when the mechanics are the same in all positions and orientations on a plane, the symmetry always induces a principal fiber-bundle structure allowing a configuration q of the system to be represented in terms of a *body frame*² pose g in the world, and a *shape* b of the robot.

The instantaneous configuration $q = (g, b)$ is an element in the overall configuration space $Q = G \times B$. The shape space B is typically a compact manifold in \mathbb{R}^k for some $k > 1$, and represents the possible shapes of the body, with the current shape being $b \in B$. The instantaneous body frame $g \in G$ is an element of the group G , which for horizontal motions is the group of rigid body motions in the plane, $SE(2)$.

Executing a cyclic shape change does not, in general,

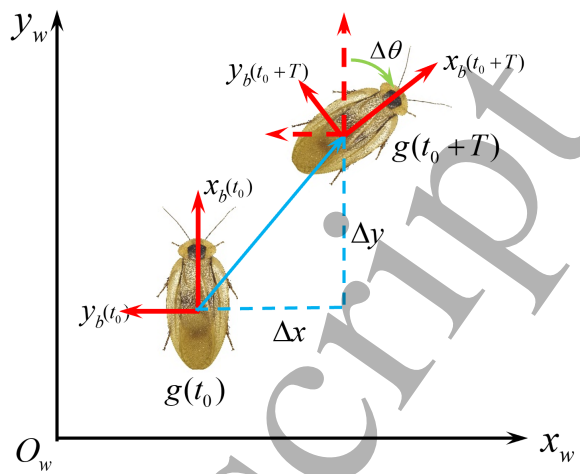


Fig. 2: Coordinate frames for definition of steering

correspond with a cycle in body frames. While the shape starts and ends the same over a cycle, the body frame changes, constituting motion.

Consider a system moving using a periodic gait with period T , and configuration given by $(b(t), g(t)) \in B \times G$. The body shape $b(t)$ must also be periodic with period T . The holonomy of this gait would be $\Delta g := g(t+T)(g(t))^{-1}$, and is the same for all choices of t . The theory of geometric mechanics tells us that $g(t)$ is completely defined by knowing $g(0)$, $\dot{g}(0)$ and $b(t)$. To capture the fact that the gait is defined by a *periodic* $b(t)$ we will take the domain of $b(\cdot)$ to be the unit circle $S^1 \subset \mathbb{C}$. Instead of thinking of $b(\cdot)$ as a function of t , we shall take $b(\phi)$, $\phi \in S^1$, and $\phi(t) = \exp(i2\pi t/T)$.

A holonomy in our case is a rigid body motion and can be represented in homogenous coordinates (see eqn. 1), where $\Delta\theta$ is the orientation change; and Δx and Δy are the translation of body frame origin as shown in fig. 2.

$$\Delta g = \begin{bmatrix} \cos(\Delta\theta) & -\sin(\Delta\theta) & \Delta x \\ \sin(\Delta\theta) & \cos(\Delta\theta) & \Delta y \\ 0 & 0 & 1 \end{bmatrix} \quad (1)$$

We define *steering* to be the ability to select the rotational component $\Delta\theta$ of the holonomy Δg within an interval around 0 by employing a one-parameter family of periodic gaits. Thus, a steering gait is a function: $b(\phi, s) : S^1 \times [-\theta_m, \theta_m] \rightarrow B$, such that the holonomy $\Delta g(s)$ for the gait $b(\cdot, s)$ has a rotational part $\Delta\theta$ equal to s . We further require that the map $\Delta g(s)$ be continuous in s , i.e. small changes in steering parameter lead to small changes in the resulting holonomy. The astute reader may note that we have omitted the discussion of T and its potential dependence on s . For now, we will assume that a steering gait has a common period T used for all choices s . However, it should be noted that if the motion is in practice “geometric”, as we will later claim, the holonomy is in fact independent of the choice of T , making this issue moot.

Steering and turning are two terms we often see used in describing locomotion. We use the terms “steer” and

² Although this may seem to be childishly obvious, defining a body frame for e.g. a slithering snake, is non-trivial and has significant computational implications [Hatton and Choset, 2011]

“turn” to refer to different phenomena: turning is the rotational component of the body frame; steering is the ability to do so continuously with magnitudes of turn in an interval containing 0 (pure translation) while at the same time also translating. Thus, one can “turn in place”, but not “steer in place”. More interestingly, a robot might have some achievable discrete translation-rotation motions available, i.e. the ability to “move and turn”, without the ability to steer. This can happen, for example, by doing two full steps on one side of the body, while taking one full step on the other side.

1.4 Phase constraints limit periodic gaits

It should be noted that repeated motions of individual legs do not, on their own, make a periodic gait. To be periodic, the motion of all legs together must be periodic. Thus, if one considers each leg as an independent subsystem executing a periodic motion, the periodicity of body motion implies a constant phase difference constraint between the “sub-system phases” [Revzen et al., 2008] of the respective legs.

To illustrate why this phase constraint has important implications, let us compare a legged system to a typical wheeled vehicle with wheels on both sides of an axle. When the vehicle turns by an angle, the left and right wheels incur a permanent phase shift representing the difference between the arc lengths travelled by the two sides. It is for this reason that wheeled vehicles have a “differential” in their axle. Because the wheels are symmetric under their axis of rotation, they are symmetric under phase change, and this phase shift is of no consequence for future motions; to the best of our knowledge its only use is the chalk marks made for parking enforcement, which use this phase difference to detect if a car has moved.

In legged systems, such shifts could produce significant changes in motion. For example, the difference between trotting, pronking, and pacing in quadruped gaits is primarily having a different, yet constant, difference between the sub-system phases of the legs [Wilshin et al., 2017]. Not only do different gaits have corresponding phase constraints, there typically are phase differences that do not generate viable gaits. For example, there can be phase differences which place no leg to support the body over a period of time, resulting in the robot body falling on the ground. To support the body, legs of a multi-legged robot must maintain their phase differences within a limited viable range. For example, many hexapods can maintain quasi-static balance by ensuring that at all times there is a set of legs contacting the ground at points which surround the horizontal projection of the Center of Mass (COM) — a constraint that can be formulated in terms of phase locking.

1.5 The geometry of steering strategies

Each periodic gait $b(\cdot, s)$ embeds the circle S^1 in the shape space B . Thus $b(\cdot, s)$ is described entirely in terms of a geometric object – its image in B , comprising a 1-dimensional collection of body shapes (see fig. 3 (a)) – and the rate at which these shapes are adopted. In those cases

where the physics create a “principal kinematic system”, that rate information has no bearing on the resulting holonomy, and the gait can be thought of as a purely geometric entity – a loop in shape space. Changing holonomy to steer must therefore require changing this loop (e.g. to fig. 3 (b)).

1.5.1 Changing timing to steer

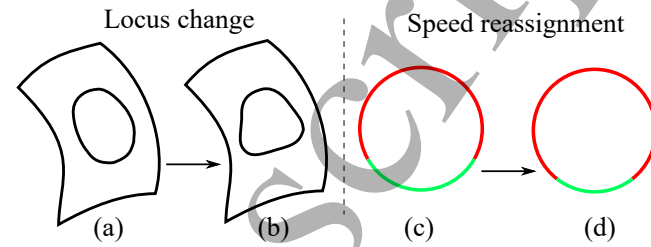


Fig. 3: Illustration of gaits and gait change. Gaits occupy a loop in shape space (a) since they are an image of the circle S^1 . To modulate a gait we may change that image in shape space (b). Alternatively, viewing a gait as a cycle (c,d) with fast (red) and slow (green) segments, a gait can be modulated by changing which parts of the cycle are executed at which speed ((c) vs. (d)).

Consider the case of a robot with 1-DoF legs. Each leg is mechanically constrained to a fixed 1-dimensional track; the only change available to such a leg is changing its timing, e.g. changing the duration it spends moving slowly vs. moving quickly in a given cycle (fig. 3 (c) and (d)). Even though the shape of the physical motion of each leg cannot change, and only its rate moving along its cycle can be modulated, this is not equivalent to being restricted to merely changing the rate of a fixed gait. The key difference is that when changing the rate of a gait, all legs change rate precisely the same way together. Even with 1-DoF legs, when the rates of individual legs along their cycles is modulated differently in different legs, the resulting shape-space loop is *geometrically* different (fig. 3 (b)). However, because of the phase constraints (see sec. 1.4) that need to be maintained, the rate modulation of individual legs must integrate to an integer number of cycles after a period. Typically, that integral will be 0, implying that all legs executed the same number of steps. While some legs can be “sped up” relative to other legs, they must then also be “slowed down” to resynchronize the legs at the end of the cycle.

1.5.2 The special case of bilateral symmetry in the plane

Consider a system (animal or robot) which is bilaterally symmetric. This implies the existence of a symmetry map $S : B \rightarrow B$ and an associated $\hat{S} : \mathfrak{se}(2) \rightarrow \mathfrak{se}(2)$ which map body shape to its mirror image, and body velocities to their mirror images. Both of these maps must be involutions, i.e. $S(S(b)) = b$ and $\hat{S}^2 = I$. Furthermore, in the case of planar motion in particular, regardless of the choice of body symmetry axis, the operator \hat{S} flips the sign on rotational velocities.

It is quite common for bilaterally symmetric organisms to employ “symmetric gaits” for translation, i.e. $S(b(\phi, 0)) = b(-\phi, 0)$ (note: $-\phi = \exp(i\pi)\phi$, the phase after a half-cycle). In such gaits the cycle of body motions consists of two mirror image halves; the first half cycle is the mirror image of the second half cycle.

The associated body frame velocities $g^{-1}\dot{g}$ satisfy $\hat{S} \cdot g^{-1}(\phi)\dot{g}(\phi) = g^{-1}(-\phi)\dot{g}(-\phi)$, i.e. they too are mirrored after half a cycle, and therefore the rotational velocities too are mirrored. In both 3D and 2D, the rotational part of motion is unaffected by translation, i.e. one can compute the total rotation of a sequence of rigid body motions without knowing the translation. This corresponds to the algebraic property of both groups being semidirect products $SE(3) = SO(3) \ltimes (\mathbb{R}^3, +)$ and $SE(2) = SO(2) \ltimes (\mathbb{R}^2, +)$. In the special case of 2D, $SO(2)$ is commutative, and therefore the rotations occurring in the second half of the gait cycle perfectly cancel those occurring in the first half, leading to a pure translation.

Thus it is a special feature of 2D planar motion (and of 2D planar motion only!) that symmetric gaits always produce a net translation with no rotation. Many organisms and robot designers employ this feature to produce translation from legged systems³.

It further follows that by introducing a parametric change in one half of the cycle, one is likely to introduce a net rotation, and that by introducing the self-same parametric change in the other half cycle containing the mirrored portion of the motion, one may introduce a rotation of the same magnitude but opposite sign. Then such parametric asymmetry makes the original symmetric gait a steering gait.

As humans it is hard for us to conceive of any other way to produce translational motion and to modulate it by steering, since bilateral symmetry is so ingrained in our morphology. Still, we must exercise caution in assuming all legged systems must use this approach. For example, horses use a “rotary gallop” gait which is not bilaterally symmetric when moving at high speeds; therefore they are likely to use non-mirror strategies for steering left and steering right.

1.6 Performance criteria for steering

Existing literature suggests different performance metrics for quantifying steering. McClung [2006] suggest the metric of $v\dot{\theta}$ that combines the angular turning rate $\dot{\theta}$ with forward speed v . This metric is dimensional, and gives a natural advantage to high-speed running robots with dynamic steering gaits. Zarrouk et al. [2015] used the metric of average heading change per step, which is estimated from the average turning rate and the step rate, to summarize the turning performance of a dozen of famous multi-legged robot platforms. We will use a similar metric – the turning angle per cycle in [deg/cyc] – and also use a geometric measure of turning, the turning radius in [mm].

³ The naive reader might assume that the translation created by a symmetric gait must be along the axis of symmetry; this is untrue. Rather, the set of translation directions achievable is itself symmetric; every gait that lists to left has a partner that lists to the right by the same angle.

Compared with the metric of turning angle per step in Zarrouk et al. [2015], turning angle per gait cycle can be applied to more cases, as the notion of “step” is only meaningful for in symmetric gaits. Typically in steering the two steps in one gait cycle have noticeably different turning angle, making turning angle per step bimodally distributed.

Turning radius is a world-frame measure which represents how sharp a turn the steering gait can achieve, and is thus an important parameter for motion planning.

2 Multi-legged steering with low DoF legs

From this section on we restrict our attention to multi-legged systems which have sufficient friction with the ground to justify the claim that COM momentum (known as “group momentum” in geometric mechanics) dissipates quickly⁴. Typically, this would be the consequence of having 3 or more point contacts with the environment at all times; if contacts can support torques, fewer contacts than 3 might suffice. Our assumption rules out discussion of highly dynamic gaits with low duty cycles, and the gaits of bipeds, and the more rapid gaits of quadrupeds.

We will discuss legs with 1 or 2 DoF, where by DoF we only include active DoF-s that can be directly controlled. Passive DoF, like the deformations of elastic legs, are not included. In this, the issues facing low-DoF multi-legged robots are the converse of those facing the typical bipedal or quadrupedal robot: the former are over-constrained with respect to the ground, whereas the latter are under-constrained.

2.1 Steering with these conditions is hard

To futher illustrate the importance of the investigation we conducted, consider the conditions for multi-legged low DoF steering. Removing any one component of “multi + legged + low DoF + steering” produces an easier to solve problem.

If “legged” is not a requirement: Many wheeled vehicle have low DoF multi-contacts with ground, but such contacts are continuous. The continuous symmetry of the wheels allows them to have arbitrarily accumulated phase from the phase difference introduced with steering. This implies that wheeled vehicles switch within an $N - 1$ dimensional family of functionally identical periodic gaits (N number of wheels), one for each possible choice of phase differences between the wheels. In that sense, wheels or treads solve a different, far easier problem.

If “multi-” is not a requirement: For bipedal robots with low DoF legs, only one leg is touching the ground for most of the time. Bipedalism creates substantial problems in controlling an under-actuated, unstable plant. For bipedal robots, the bigger challenge is to maintain heading and stability – a single pin-joint contact, or even a toe and heel pair of contacts, often generate heading and orientation changes that can be exploited for steering. It should also be mentioned that

⁴ By “quickly” we mean that we are in the domain where the recent results of Kvalheim et al. [2019] apply, implying that the equations of motion can be written in an approximately geometric form (*ibid*).

1 with only two legs, 3 DoF per leg requires only 6 motors, i.e.
 2 a device of comparable mechanical and electrical complexity
 3 to a hexapod with low DoF legs.

4 If “low-DoF” is not a requirement: As soon as each leg
 5 has 3 or more DoF, foot placement can be arbitrarily con-
 6 trolled within a volume, making the body frame fully locally
 7 controllable in a kinematic sense. At the cost of this extra
 8 complexity, steering becomes much easier, at least at the low
 9 speeds we consider here.

10 It is also important to notice that these conditions do not
 11 make locomotion uniformly difficult; we have only identified
 12 these difficulties in the case of steering. If the robot is not
 13 required to allow the heading to be continuously controlled
 14 while moving, making the robot bilaterally symmetric allows
 15 one to exploit the trick described in section 1.5.2 to translate
 16 without rotation. In particular, in the case of hexapod robots,
 17 a designer may use the alternating tripod gait. In such a gait,
 18 the three feet in contact with the ground form a triangle under
 19 the center-of-mass and translate relative to the body without
 20 changing the shape of the triangle. This uniquely defines
 21 the motion of the body frame, and given bilateral symmetry,
 22 allows for a walking gait with zero heading change.

23 From these examples, we can see that multi-legged
 24 steering with low-DoF legs is particularly hard. Solving this
 25 problem would allow us to use multi-legged robots with a
 26 mechanical and electrical complexity lower than that of to-
 27 day’s popular bipeds and quadrupeds.

29 2.2 1-DoF steering creates conflicting constraints

30 To be able to translate using a set of non-slip foot con-
 31 tact, those foot contacts must themselves translate as a rigid
 32 set of points in the body frame while in stance. This geo-
 33 metric constraint must be designed into the motion of any set
 34 of legs used for non-slip motion. Note that this geometric
 35 constraint is necessary, but not sufficient to make a gait have
 36 no slip: accelerations or gravitational force components can
 37 be large enough to break a contact outside its friction cone
 38 and cause it to slip anyway. The gaits we describe are slow
 39 enough, and stable enough where all slipping is caused by
 40 incompatible foot motions.

41 The problem of incompatible foot motions becomes
 42 starkly clear when considering a robot with 1-DoF legs (see
 43 fig. 4). The feet of 1-DoF legs follow a 1-dimensional path
 44 in the body frame. Whichever feet support the body while
 45 translating (we assume a tripod in fig. 4), they must follow
 46 identical paths in the body frame. Whichever feet support
 47 the body while steering along some arc, the feet must follow
 48 different paths from each other because they are at different
 49 radii from the center of rotation. Since the legs are assumed
 50 1-DoF, each individual leg can only follow one path – show-
 51 ing that allowing a range of turning radii creates conflicting
 52 constraints on the 1-DoF path of the feet.

53 Naively, one might assume that hexapedal robots with
 54 1-DoF legs moving parallel to the body would have trouble
 55 steering and turning. In practice, direction changes merely
 56 force the robots break the non-slip constraint. For example,
 RHex is highly maneuverable [Johnson, 2013] and turns eas-

ily, but it does so with considerable slipping.

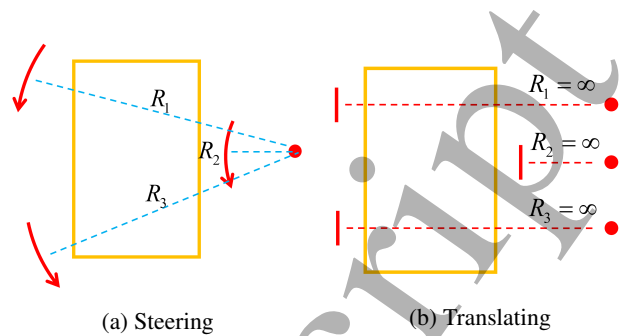


Fig. 4: Leg strokes in the body frame for a tripod of legs, assuming non-slip motion while steering (4a) and while translating without heading change (4b). Note that leg strokes needed for non-slip steering and noslip translation have incompatible 2D projections in the body frame, and thus cannot be the result of the same 1-DoF motion.

3 3 Results: low-DoF hexapods steer with slipping

To verify our analysis about low-DoF multi-legged steering and measure slipping behavior during steering, we used two types of robot platforms that have different morphology and different effective DoF per leg (1-DoF and 2-DoF) for our experiments. We tested both robots on two substrates – a relatively slippery linoleum floor, and higher friction interlocking rubber tiles (C9 interlocking fitness mat; Target Inc 2015). We tried a variety of steering parameters and speeds. All the locomotion results were recorded using a reflective marker motion tracking system (10 Qualisys Oqus-310+ cameras at 120 fps, running QTM 2.17 build 4000, interfaced to custom SciPy 0.17.0 code using the Qualisys 1.9 Realtime API)

3.1 BigAnt 1-DoF hexapedal robot



Fig. 5: BigAnt

Our 1-DoF robot tests were conducted on the BigAnt robot. The design and development of BigAnt is outside the scope of this paper, and only summarized briefly here. Its chassis structure and mechanisms were manufactured using the PARF (plate and reinforced flexure) technique [Fitzner et al., 2017; Miller et al., 2015] developed in our lab. Using PARF, the chassis of BigAnt can be manufactured with minimal tooling (a knife) and less than US\$20 worth of materials (Elmers Products Inc. foam board $508 \times 762 \times 7\text{mm}$ and 3M Scotch #8959 fiber tape). With a laser cutter instead of the knife, the chassis can be fabricated within 7 hours, which includes 30 minutes assembly. The fast and inexpensive turnaround allowed the design of BigAnt to be iterated quickly. Instead of simulating each re-design we used experiments to directly measure and iteratively improve the robot (see fig. 5 for version used here).

Like the RHex family of robots [Galloway et al., 2010; Saranli et al., 2001], BigAnt has six 1-DOF legs. Each leg is actuated by a servo motor (Robotis Dynamixel MX64), but rather than directly rotating a leg like RHex robots do, the legs of BigAnt are driven through a 4-bar mechanism. The leg trajectory was chosen by exploring the space of possible 4-bar designs for motions with a flattened backward stroke and a high clearance when swinging forward (see fig. 6a). While other linkages exist that could produce a flatter back stroke, those require significant additional complexity or larger dimensions compared with current 4-bar design. The BigAnt leg is highly modularized, making it easy to both replace worn out legs, and install custom leg geometries for different applications.

3.1.1 BigAnt steering gaits

While the 4-bar linkage defines the geometry and position-dependent gearing ratio of BigAnt legs, the instantaneous position of the leg along its ovoid path is under (conventional PID based) servo control. If all six legs are driven at constant angular speed as two anti-phase tripods of legs (“left tripod” FL-MR-HL containing [F]ront-[L]eft, [M]iddle-[R]ight and [H]ind-[L]eft legs; and the “right tripod” FR-ML-HR), the robot exhibits substantial up-down motions representing parasitic work against gravity. To obtain a smoother motion, we scheduled the motion of the shaft angles ψ_k $k \in \{\text{FL}, \text{FR}, \text{ML}, \text{MR}, \text{HL}, \text{HR}\}$ as a function of leg phase ϕ_k using a two-speed schedule: a (typically) fast “aerial phase”, and a (typically) slow “ground contact phase” (see fig. 7). To our knowledge, this idea comes from work done by M. Buehler on the RHex robot, and is sometimes referred to as a “Buehler Clock” in the RHex literature. The Buehler clock is defined by 4 parameters. Often these are the “sweep” angle through which the leg moves in ground contact, a “duty cycle” defining the fraction of the cycle in ground contact, the stance angle “offset” away from vertical, and the phase at midstance. Because the choice of zero phase is arbitrary, we always chose the liftoff phase to be 0, leading to a Buehler clock defined by only 3 parameters.

We designed our gaits by tweaking these three gait parameters at a moderate gait frequency ($\sim 0.2\text{Hz}$) until the

robot was both moving reliably and hardly bouncing up and down. We then introduced steering control by modulating the functions ψ_{ML} and ψ_{MR} with a steering input s . The overall phase change of such a modulation must be 0; it is therefore a periodic function of phase. We chose an obvious candidate – $\cos(2\pi\phi)$ which we used to advance/retard the phase of one middle leg, and retard/advance the phase of the other middle leg in an anti-symmetric way. Letting $b(\phi) : \phi \mapsto \psi$ be the Buehler clock function chosen, our shaft angles were:

$$\begin{aligned}\psi_{\text{FL}} &= \psi_{\text{HL}} := b(\phi) \\ \psi_{\text{FR}} &= \psi_{\text{HR}} := b(\phi + 1/2) \\ \psi_{\text{ML}} &:= b(1/2 + \phi + sk_s \cos(2\pi\phi)) \\ \psi_{\text{MR}} &:= b(\phi - sk_s \cos(2\pi\phi))\end{aligned}\quad (2)$$

where $k_s := 0.24$ is a constant gain adjusting sensitivity. The shaft angles with steering modulation of $s = 0.55$ are shown in fig. 7. The corresponding leg trajectories at fig. 6b and fig. 6c give us an explicit view of how the mid right leg is slowed down at ground contact and how the mid left leg is sped up at the same part of trajectory. With such modulated tripod gait, we can now steer BigAnt by changing the input parameter s to different values.

The strategy of steering by modulating middle legs is itself bio-inspired, and based on the strategies cockroaches often use for turning [Jindrich and Full, 1999].

3.1.2 BigAnt steering gait test results

We tested the steering gait introduced in the previous subsection on BigAnt with different steering input parameters and recorded the motion using Qualysis motion capture systems. Fig. 8 shows an example of BigAnt walking on our lab floor; we provide detailed plots and statistics for this trial which consisted of 6 strides at gait frequency $f = 0.22\text{Hz}$ and steering input $s = 0.75$. Results from other trials were quite similar, and so we do not provide such details from every trial. We collected a total of $N = 39$ trials, $N_s = 225$ strides, total time of ~ 1800 seconds at 120fps for a total of $N_f = 2.16 \times 10^5$ frames of data, using $N_r = 3$ similarly constructed robots.

Additionally, we collected various metrics of slipping: (1) the slipping distance; (2) the “slipping ratio” of slipping distance to total leg motion distance. A slipping ratio of 0 indicates a non-slip gait; a slipping ratio of 100% represents a leg that always remains in contact with the ground and is never in static friction. The average slipping ratio for the trial (fig. 8) we examined in details is 20.6%. To better understand the kind of slipping taking place, we separate slip into two components: slipping in the direction tangent to the arc the robot is moving along, and slipping in the direction radial relative to this arc. For the slip in each components, we compute both the time-averaged absolute value, and the time-averaged value (see table 1).

We also examined the foot motions with respect to the body frame. Our expectation was that foot motions are, for

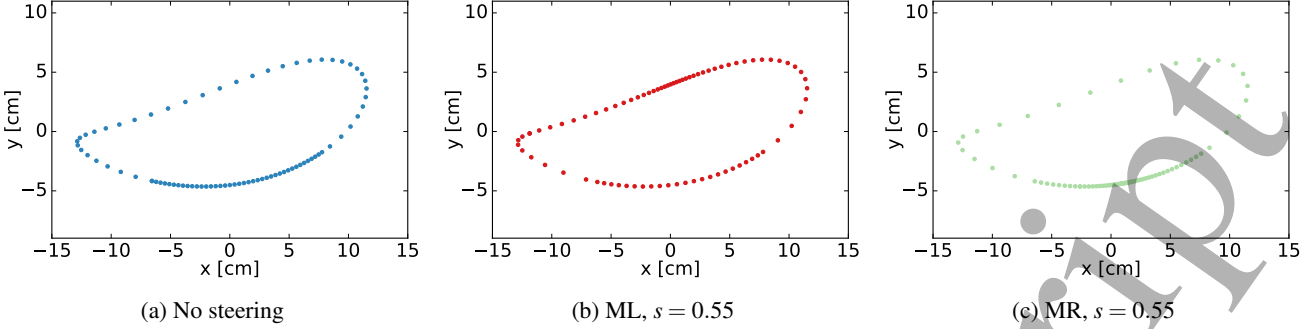


Fig. 6: Leg trajectory in the body frame, with points indicated at equal phase intervals. Without steering (a) a clear Buehler clock effect is visible. With steering at $s = 0.55$, the timing of ML (b) and MR (c) becomes different, even though the shape of the trajectory is the same.

Table 1: Slipping by leg for $s = 0.75$, $f = 0.22$ Hz. Motion capture error bounds were ± 3.5 mm at 99th percentile of error

	FL	ML	HL	FR	MR	HR	Mean
Slip/cyc [mm]	98	48	119	115	60	133	95
Slip ratio [%]	18.7	9.6	22.1	28.7	13.8	30.9	20.6
Abs. tangent [mm/cyc]	45	40	66	97	52	96	66
Abs. radial [mm/cyc]	79	18	81	49	20	77	54
Avg. tangent [mm/cyc]	-9	26	31	25	-5	35	17
Avg. radial [mm/cyc]	-47	5	44	-12	2	38	5

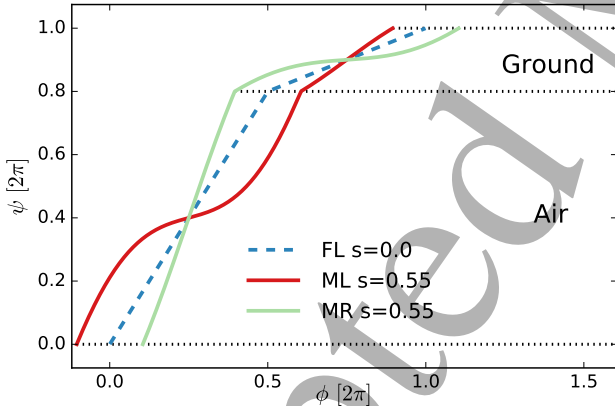


Fig. 7: BigAnt joint angle output as a function of local phase ϕ within a gait cycle. When moving straight, the phase to joint angle relationship is a “Buelher clock” consisting of a fast constant speed phase for aerial motion and a slow constant speed phase during expected ground contact(dashed blue line). With a steering input of $s = 0.55$ (see eqn. 2), the mid left leg motion (red) and mid right leg motion (green) are modulated in opposite ways, generating a steering motion to the right.

(image) legs we observe, we should see the same trajectory for the foot in the body frame (see fig. 9(b)(c)(d)).

To get more details about how the interaction between leg and ground results in such steering behavior, we plotted world frame z motion vs. body frame x (see fig. 9(a)(e)). These two subfigures show a longer stroke in ground contact for all left legs, compatible with the observation that the robot turned to the right.

3.1.3 BigAnt turning rate results and slipping results

At this point it should become quite clear that while Bi-gAnt is not hard to steer with our choice of steering gait (see fig. 8 for steering with different inputs of s), the actual mechanical interaction that produces steering from the modulation of ψ_{ML} and ψ_{MR} with s is not at all obvious.

To better understand how BigAnt actually steers we conducted a multi-robot, multi-parameter study, summarized in fig. 10. We compared the results taken from 3 independently constructed copies of the BigAnt robot, over a variety of gait frequencies, and on both low friction and high friction substrates. The purpose of this comparison was to establish whether it was in fact s which controlled the steering behaviors, or whether we merely created systems whose multi-contact interaction too complex for us to understand in some idiosyncratic way.

Since the experimental datasets are of slightly different sizes, and there is no reason to assume the parameters we

Since the experimental datasets are of slightly different sizes, and there is no reason to assume the parameters we

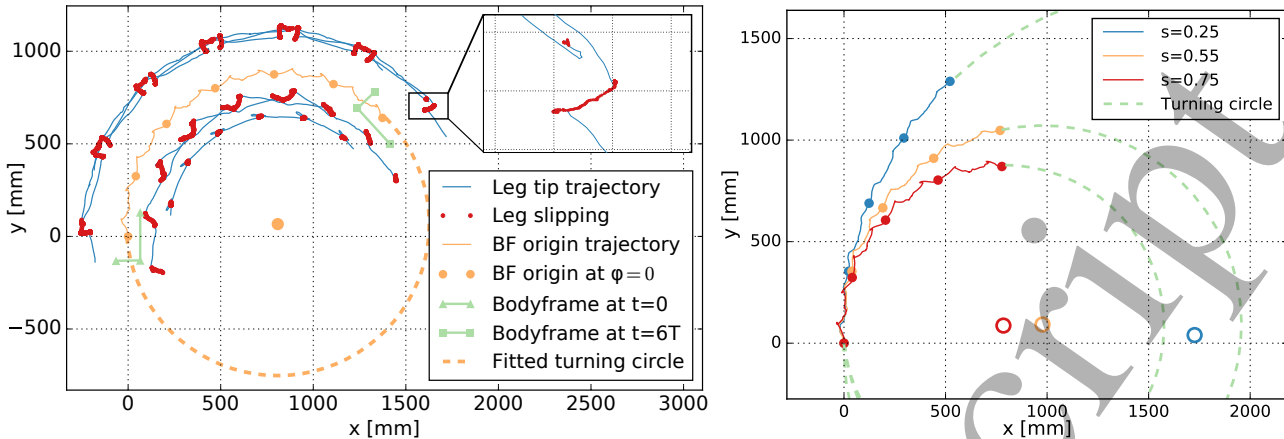


Fig. 8: BigAnt motion in world frame (left) and Steering results at different values of s (right). For gait frequency $f = 0.22\text{Hz}$; steering input $s = 0.75$, we plotted (left) leg tip trajectories (blue), with slipping highlighted (red dots; magnified in inset), and the trajectory of the body frame origin O (yellow line) with the beginning of cycle indicated (yellow dots). We indicated the markers that define the body frame (light green) at the beginning (triangles) and end (squares) of this 6 stride trial. To estimate turning radius we fit a circular arc (dotted yellow) to the body frame origin. In this trial, BigAnt turns $23^\circ/\text{cyc}$ and the turning radius is 818 mm. Exploring other values of s (right) we plotted the motion of the body frame origin at different values of the steering parameter s (teal, yellow, red for 0.25, 0.55, 0.75 resp.), while leaving all other gait parameters unchanged. To each trial of 4 strides we fitted a circular arc (dashed green) and indicated the center of rotation (teal, yellow, red circles). Results suggest a clear parametric dependence of turning radius on steering parameter value.

measure are normally distributed, we used non-parametric methods for our statistical analysis. Each grouping of parameters was represented by a bootstrap sample of size 1000; this size was chosen because all groupings were at least of this size. The use of bootstraps facilitates homoscedasticity of the box-plots we use to represent the results, and allows the spread to be meaningfully compared across groupings. The results show that s reliably governed steering across all 3 robots, and produced statistically indistinguishable outcomes with them. They further show that once the influence of s is removed, neither gait frequency nor substrate friction have a detectable influence on the rate of turning. This suggests a very peculiar physics: one that is geometric by its independence from time parameterization, includes significant slipping, and yet is nearly independent of the magnitude of the friction coefficients that govern this slipping.

To gain further insight into how such a counter-intuitive outcome might appear, we analyzed several slipping metrics of individual legs at different values of the steering parameter s , holding the remaining parameters constant. These results are in fig. 11, and come from the $f = 0.22\text{Hz}$ trials with robot R1.

From fig. 11a we observe that the slip ratio, which equals total distance slipped divided by total distance traveled, clearly increases with s . The change is expressed mostly in the tangent direction, where legs of the left tripod (FL,MR,HL) are retarded more with higher s , and legs of the right tripod (FR,ML,HR) are advanced. These changes are straight-forward to anticipate from eqn. 2. The radial directions harbors a surprise: FL and HL respond to changes in s quite strongly and with opposite sign, but their symmetric counter-parts FR and HR do not. This suggests that during

left tripod stances with large s , FL moves radially in (right) and HL moves radially out (left), whereas in right tripod stances little to no radial motion is observed.

3.2 MechaPod 2-DoF hexapedal robot

To explore the relationship of slipping and steering with 2-DoF legs, we used the “MechaPod” robot, a hexapedal robot driven from a previously studied “centipede robot” [Sastra et al., 2012, 2008]. Centipede attempted to be the first modular robot to exhibit a dynamic gait with aerial (ballistic) phases using geared-down, conventional servo motors. MechaPod consists of an articulated spine with 7 motor modules, connected to 3 elastic legs that extend side-to-side (see fig. 12).

Defining a body frame for shape-changing robots can be a non-trivial [Hatton and Choset, 2011]. Following previous work [Sastra et al., 2012], we associate a body frame with MechaPod by taking the line connecting the center of one end-module (“front”) with the center of the opposite end-module (“back”) as the X axis, and constraining the center of the middle module to the Y axis. With respect to this body frame, each of the robot’s feet can be thought of as under 2-DoF control: one “yaw” DoF coming from the adjacent Z -axis motor(s) on the spine, and one “roll” DoF coming from the X -motor to which the leg is attached. The remaining 1-DoF that is unaccounted for allows the spine to roll with respect to the ground without moving the legs.

3.2.1 MechaPod non-slip steering gaits

We considered the problem of introducing steering into the alternating tripod gait used for rapid motion with the

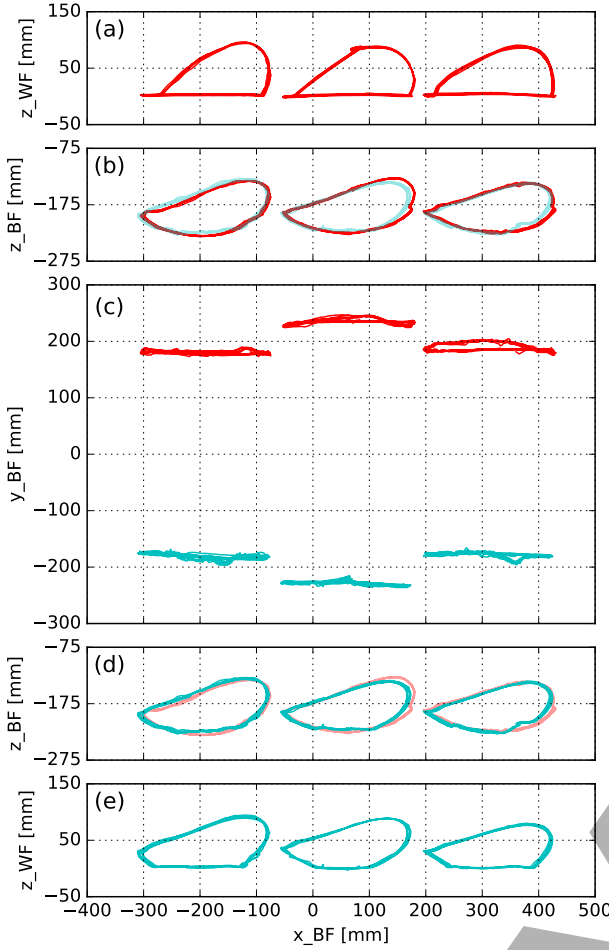


Fig. 9: BigAnt foot motion in the body and world frames. We show horizontal (x, y) projection (c) and sagittal (x, z) projections (a)(b)(d)(e) with side of the leg indicated by color (left - red; right - teal). In the body frame (b)(d), the contralateral leg is also shown (transparent) to highlight that motions are symmetric in the body frame. Viewed with world frame z (0 is ground), the left legs (a) have a longer ground stroke than the right legs (e). This highlights the counter-intuitive notion that actual ground strokes can be quite different even with identically shaped trajectories, thanks to timing and slipping.

Mechapod. When engaging in this gait, the roll motors in the front, middle, and hind modules are typically set to the same fixed angle with alternating signs. Under the assumption that this angle is small, its cosine is nearly constant. This allowed us to plan the motion of the 3D robot in terms of its 2D horizontal projection, which consists of two 4-bar linkages tied together. Each 4-bar has one DoF allowing the robot to move while maintaining non-slip contact with the ground. The idea of embedding such a 4-bar linkage to allow non-slip motion was an insight of the original “centipede robot” designer (S. Sastra et al., 2008); see fig. 13).

We construct a periodic 4-bar gait as follows (refer to fig. 14). Assuming a cycle with period T , we take $t = 0$ as start of support for one tripod, and $t = T/2$ as switch to

support by the other tripod. At time $t = T$, the robot configuration needs to cycle back to the same configuration as that at time $t = 0$ to have a periodic solution, so distances between foot locations must satisfy $|AB(0)| = |AB(T)|$ and $|A'B'(0)| = |A'B'(T)|$. With the non-slip constraint, the supporting legs are pinned to the ground. During the first step ($0 \leq t \leq T/2$), feet A, B are on the ground; during the second step ($T/2 \leq t \leq T$), feet A', B' are on the ground. Thus $|AB(0)| = |AB(T/2)|$ and $|A'B'(T/2)| = |A'B'(T)|$; together with the previous equalities, this gives:

$$|AB(0)| = |AB(T/2)| \quad |A'B'(0)| = |A'B'(T/2)| \quad (3)$$

Assuming we start a step with $[\beta(0), \psi_2(0), \psi_3(0)]$ at $t = 0$, and by definition $\beta(0) := 0$, the 4-bar structure dictates the distances $|AB|$ and $|A'B'|$ as a function of β , and through $\beta(t)$ as a function of t . The solution of eqn. 3 thus uniquely selects possible values of $\beta(T/2)$ as an implicit function of the initial $\psi_2(0), \psi_3(0)$. This implies that by exhaustively scanning choices of these initial values we can discover all possible non-slip Mechapod gaits. We performed such an analysis, showing $\beta(T)$ as a result of initial values $\psi_2(0), \psi_3(0)$, also taking into account to forbid poses that would cause self-interference (see fig. 15). The maximal turning rate this analysis predicted was $8.09^\circ/\text{cyc}$, given the dimensions of the physical Mechapod.

We tested the maximal non-slip turning gait going forward and back on the robot (total of $N = 34$ trials, $N_s = 136$ strides, $N_f = 6.12 \times 10^4$ frames of data; see one such trial in fig. 16). Going forward, the robot averaged $6.7^\circ/\text{cyc}$ turning, and going back $9.6^\circ/\text{cyc}$. Thus, on average this gait produced $8.15^\circ/\text{cyc}$ of turning while steering – a very close correspondence to the theoretical prediction of $8.09^\circ/\text{cyc}$. The turning angle difference between forward and backward motion comes from the fact that Mechapod is not perfectly symmetric. Examining the foot motions in the robot body frame (see fig. 17) shows that right tripod stance trajectories closely follow the concentric arcs expected from the theoretical analysis in fig. 4, whereas left tripod stance motions are far less arced. The robot turned strongly to the left in right tripod steps, and then turned a little back to the right in left tripod steps.

We note an additional complication of using this method to produce non-slip steering: to steer we need a parametric family of gaits controlled by a steering parameter $-1 \leq s \leq 1$ (here ± 1 chosen as limits wlog). This requires being able to solve $\psi_2(t, s)$ and $\psi_3(t, s)$ such that for every value of s we obtain a non-slip motion – thus solving the 4-bar kinematics in real-time. We must then also choose a family of non-slip gaits such that $[\psi_2(0, s), \psi_3(0, s)]$ traces a path from the extremal left turn at $s = -1$, through a no-turning gait at $s = 0$, and finally to e.g. $s = 1$ for the extremal right turn. Ideally, this path should be chosen such that the turn angle is proportional to s . While of these additional steps are straightforward to implement, the goal of the current investigation was to compare non-slip steering and steering which

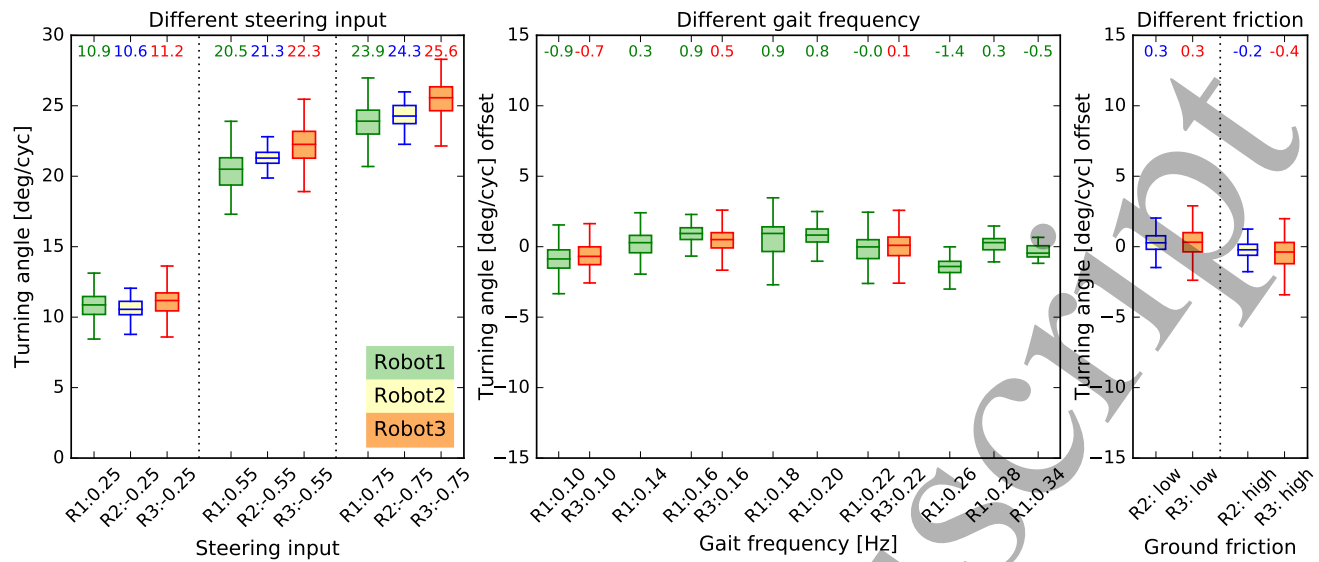


Fig. 10: Turning rate dependencies on various parameters. To show dependence (or lack thereof) of turning rate on various parameters, we binned data according to the parameter value and collected a bootstrap sample of size 1000, making the spread of the various box-plots meaningful for comparison. We also present the numerical mean values of each box plot (number above box-plot). First, we group data by which of the 3 comparable robots (R_1 , R_2 , R_3 ; green, yellow with blue frame) we took data from, and at what value of the steering parameter s that trial was running (0.25, 0.55, 0.75 parts of the left subplot). Results show a clear dependence of turning rate ω on s , which is consistent among all 3 robots. Since the influence of s and robot ID r dominated variability in ω , we subtracted the average $\langle \omega \rangle(s, r)$ from ω to examine the data for any additional effects of gait frequency (0.10 Hz to 0.34 Hz middle subplot), or ground-to-foot friction coefficient (right subplot). Results fail to reject the null for these potential influences. Together, these results suggest that s alone governs the turning rate for each robot, and does so reliably for all the robots of this type we built.

employs slipping.

3.2.2 Mechanopod steering gaits with slipping

As an alternative to producing a non-slip steering gait, we explored steering the tripod gait with various modulations. The gait we employed was of the form:

$$\begin{aligned} \psi_1 &= -\psi_4 = \psi_7 := A_{\text{roll}} \sin(\phi) \\ \psi_2 &= -\psi_6 := A_{\text{yaw1}} \cos(\phi) \\ \psi_3 &= -\psi_5 := A_{\text{yaw2}} \cos(\phi) \end{aligned} \quad (4)$$

We then introduced two types of modulation “spine twist” where all roll motors were given a constant offset to the same side causing the robot to lean to one side, and “spine bend” where all yaw motors were given a constant offset to the same side causing the neutral shape of the spine to be bent along an arc (see fig. 18). These modulations were introduced as follows: the updated motor angles $\psi'_i(\phi, s)$ were given by $\psi'_i(\phi, s) = k_{\text{twist}}s + \psi_i(\phi)$ for $i \in \{1, 4, 7\}$, and $\psi'_i(\phi, s) = k_{\text{bend}}s + \psi_i(\phi)$ for $i \in \{2, 3, 5, 6\}$. This allowed us to introduce various combinations of bending and twisting, and test their efficacy at producing steering.

As expected, making either k_{twist} or k_{bend} non-zero produced reliable steering gaits. We presented various combinations of bending and twisting in [Zhao and Revzen, 2016; Zhao et al., 2015]. The effect of bending ($k_{\text{bend}} > 0$) followed intuition quite well – when the spine was bent, the

robot turned around a center of rotation on the inside of the average arc of the spine (although not around the center of the spine’s arc). Twisting ($k_{\text{twist}} > 0$) produced even better steering performance, where leaning to the left caused the robot to steer right; the mechanism of this steering result remains somewhat unclear.

Table 2: Steering and slipping results for trials in fig. 20. Slip in this table are averaged by leg then by gait cycle.

$s [^\circ]$	$^\circ/\text{cyc}$	$R [\text{mm}]$	Slip [mm/cyc]	Slip ratio
10	8.1	1802	129	26.5%
20	14.2	1312	133	26.9%
30	22.3	860	138	29.2%
60	32.8	437	186	36.2%

We investigated the twist-based steering gait for the Mechanopod using similar analyses to those used for BigAnt (see figs. 20, 19, and 20). Table 2 gives the corresponding quantitative steering performance and slipping metrics.

The largest twist steering parameter we used was $s = 60^\circ$. With this value, the Mechanopod turned approximately $33^\circ/\text{cyc}$, about $\times 4$ better than the best non-slip steering per-

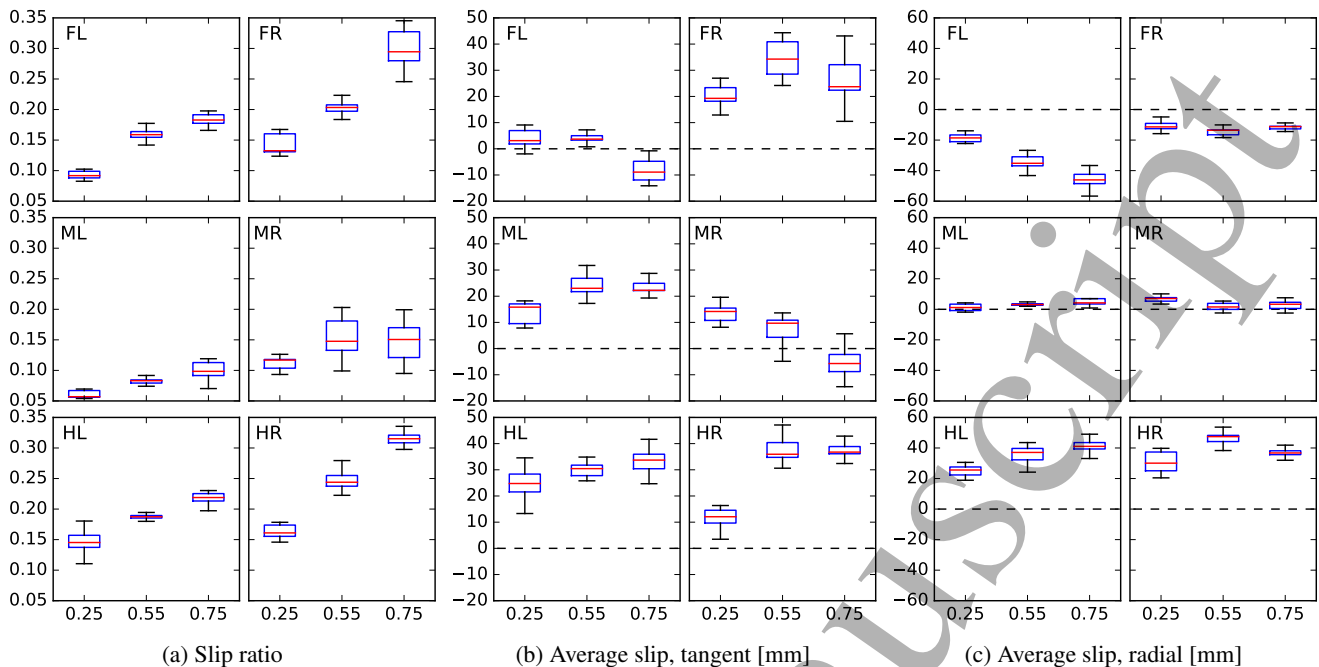


Fig. 11: BigAnt slipping metrics, by leg and steering parameter value. We collected the slipping metrics for BigAnt platform R1 with $f = 0.22\text{Hz}$, partitioned by $s = 0.25, 0.55$, and 0.75 . We present the ratio of slipping distance to travel distance (a); average distance slipped tangent to direction of motion along the turning arc (b); and average distance slipped radial to turning arc and thus perpendicular to direction of motion (c). Slipping in (b) is non-productive for locomotion; slipping in (c) is necessary to rotate the robot around its axis. Each metric is presented separately for each of the robot's legs. We created each box-plot by evaluating the metric by a bootstrap sample of 100 period-long windows from the relevant slice of the dataset. Note that with this gait the robot arcs to the right.

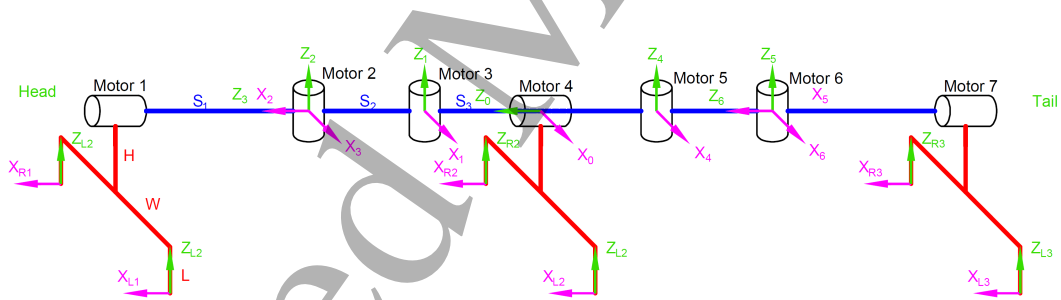


Fig. 12: Mechapod is actuated by 7 highly geared down servo motors (Dynamixel MX106 and MX64); 4 of them are on the spine controlling the spine yaw motion (Motor 2,3,5,6); the other 3 controls leg roll motion (Motor 1,4,7). The 3 pairs of legs are coupled by spring steels which offer compliance to the robot.

1 formance. This turning rate is far better than BigAnt and the
2 robots investigated by Zarrouk et al. [2015]. It is also worth
3 noting the slip ratios at approximately 36%, almost double
4 that of cockroaches.

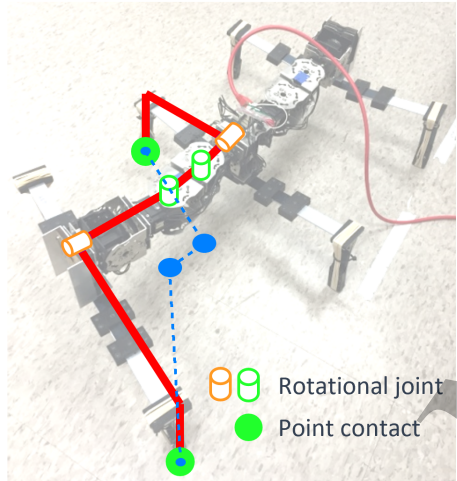


Fig. 13: Overlay showing how Mechapod contains a 4-bar linkage. When the roll motors (orange cylinders) are activated and holding stationary at equal angles, the robot can be standing on a tripod (here FL,MR,HL) with presumed point contacts at the feet (green dots for FL,MR). The projection of the robot on the horizontal is then a 4-bar linkage (blue dots and dashed lines).

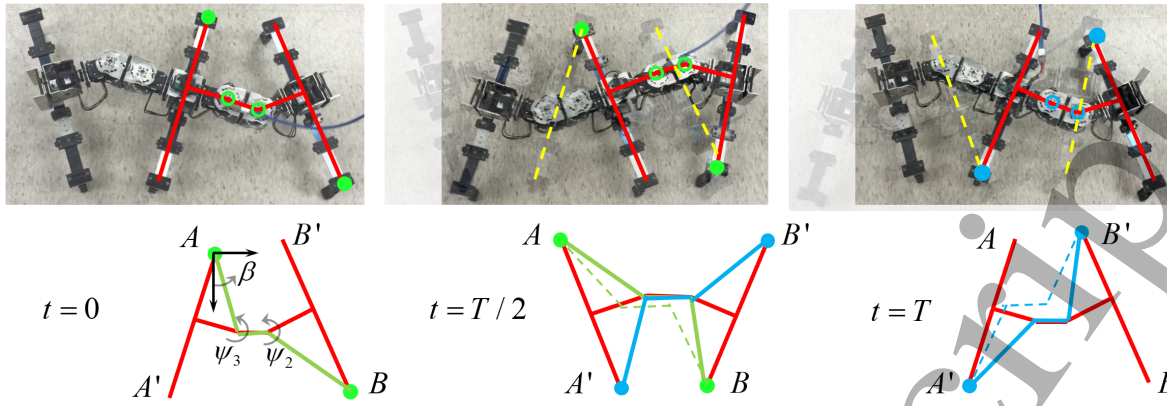


Fig. 14: Mechapod locomotion can be represented by the motion of two 4-bar linkages. We show 2 consecutive steps of Mechapod walking left to right (top row; 3 photos of double stance configuration). We indicate the skeleton of the front half (red lines; open circles for motors) and the previous leg positions (dashed yellow). Supporting legs in first step (solid green circles) and in second step (solid blue circles) show the pivots of the abstracted 4-bar (bottom row). The first step 4-bar (green) and the second step 4-bar (blue) share link lengths and there is a well defined relationship between the angles of the links before and after the support switch for a fixed value of spine motor angles ψ_2, ψ_3 . We denote the locations of the feet by A, B, A', B' , and by β the sweep angle of the $A-A'$ leg. Since this is a kinematic model, we may arbitrarily choose the switchover time to be mid-cycle at $t = T/2$.

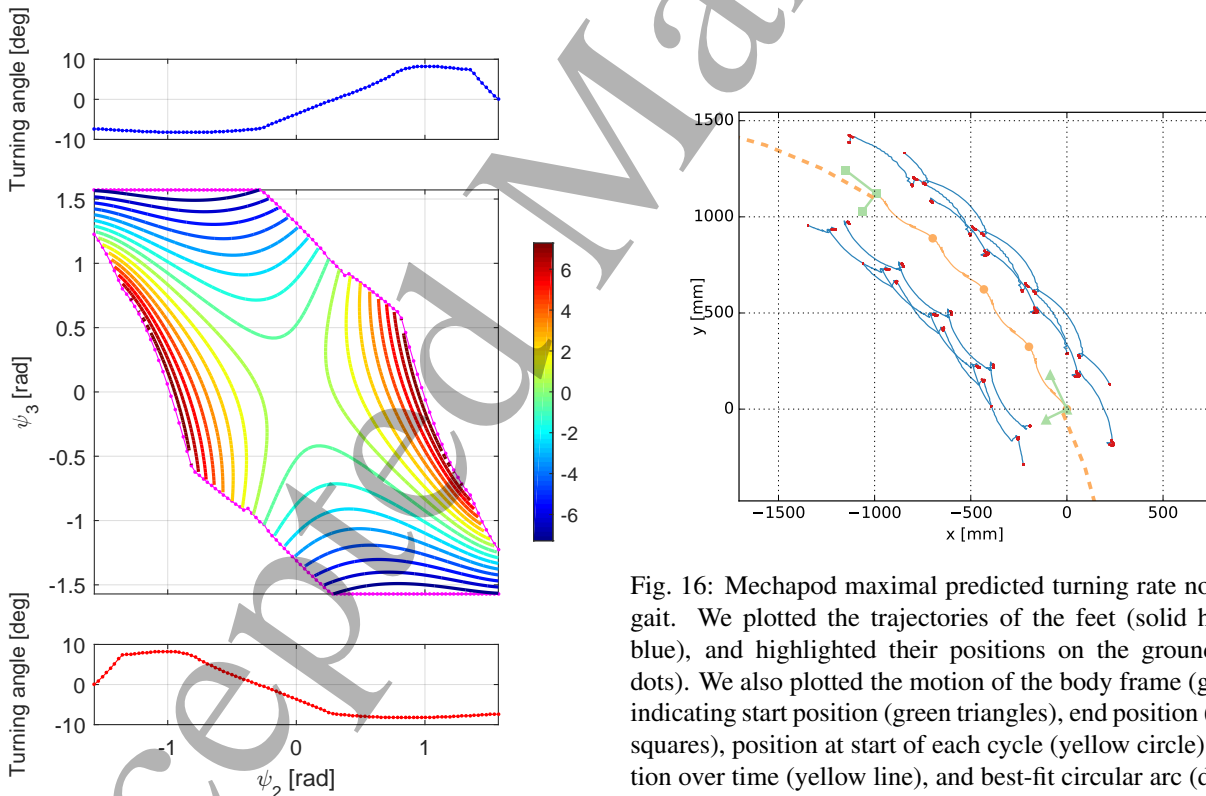


Fig. 15: $\beta(T)$ for all non-slip gaits of Mechapod. The overall turn $\beta(T)$ (colored contours, center subplot) after a cycle of non-slip motion for feasible non-slip gaits, and its value on the two boundaries of the feasible range (magenta dots in center; top and bottom graphs), which also show the extremal values.

Fig. 16: Mechapod maximal predicted turning rate non-slip gait. We plotted the trajectories of the feet (solid hairline blue), and highlighted their positions on the ground (red dots). We also plotted the motion of the body frame (green), indicating start position (green triangles), end position (green squares), position at start of each cycle (yellow circle), position over time (yellow line), and best-fit circular arc (dashed thick yellow line).

The robot walked 4 cycles at a frequency of 0.33Hz. Results show that feet do in fact hardly slip at all.

In this trial, Mechapod turns $8.0^\circ/\text{cyc}$ and the turning radius is 2692mm

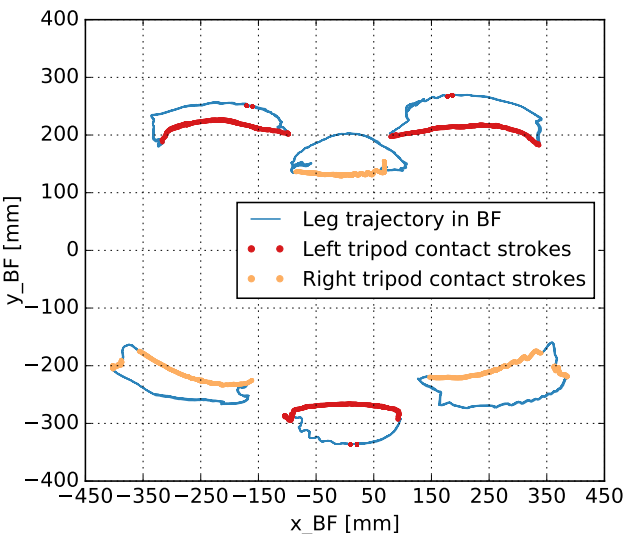


Fig. 17: MechaPod body frame foot motions from the trial shown in fig. 16. Robot moves to the right. We determined ground contact frames based on the vertical height of the feet from motion tracking. Since the legs are highly elastic, the feet did bounce in and out of contact as shown.

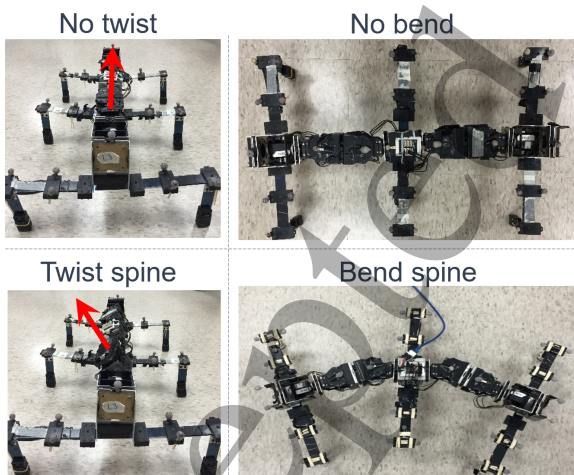


Fig. 18: MechaPod neutral position and its modulation for steering. When the MechaPod is moving without turning, its shape oscillates around the shapes shown in the top row. By adding spine twist, the spine leans on average (bottom left); by adding spine bend, the spine is arched on average (bottom right).

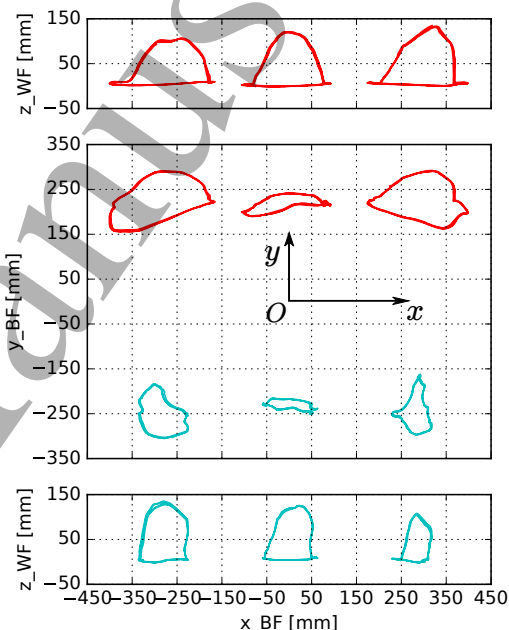


Fig. 19: Foot motions in body frame x,y and world z for trial in fig. 20. We plotted the motion of the left legs (top subplot, red in middle subplot), and the right legs (bottom subplot, teal in middle subplot). The twist-based steering gait produced shorter ground strokes on the right than on the left, commensurate with a turn to the right.

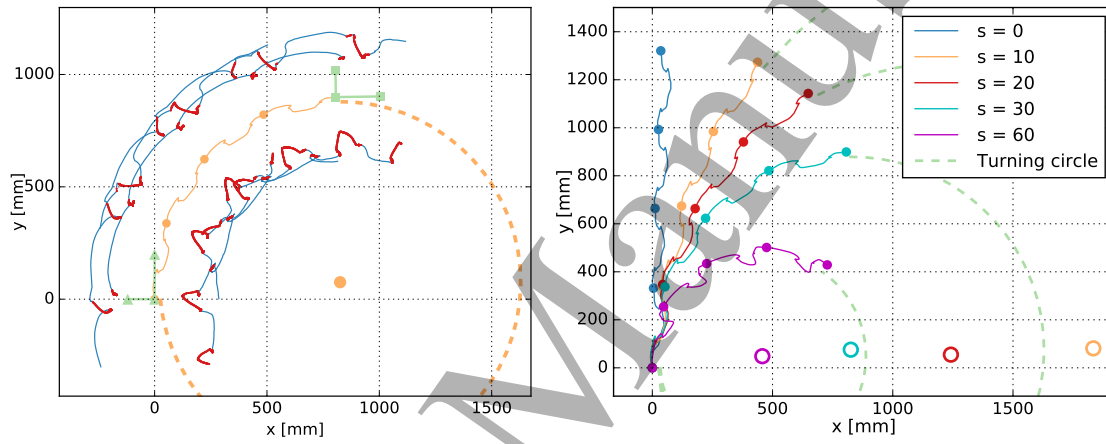


Fig. 20: Mechapod motions with $k_{\text{twist}} = 1, k_{\text{bend}} = 0, s = 30^\circ$ (left) and twist gait on low friction surface, for $s = 0, 10, 20, 30, 60^\circ$ (right). We plotted the trajectories of the feet (solid hairine blue), and highlighted their positions on the ground (red dots). We also plotted the motion of the body frame (green), indicating start position (green triangles), end position (green squares), position at start of each cycle (yellow circle), position over time (yellow line), and best-fit circular arc (dashed thick yellow line). The robot walked 4 cycles at a frequency of 0.33Hz and turned $22.3^\circ/\text{cyc}$, for a turning radius of 860mm. Results show that feet slipped a great deal. For other values of $s = 0, 10, 20, 30, 60^\circ$ we plotted (right) location of body frame (solid) with COM after each cycle (solid circles), best fit turning arc (green dashed) and center of rotation (open circle).

1 4 Conclusion and discussion

2 Multi-legged robots are not in common use, despite their
 3 inherent stability and the mechanical robustness that can be
 4 achieved with three or more legs contacting the ground at
 5 once. Two factors that might be limiting their deployment
 6 are the mechanical complexity of building many multi-DoF
 7 legs, and the difficulty in understanding and planning for the
 8 multi-contact regimes that arise when these robot morpholo-
 9 gies are employed. The first factor can be addressed by using
 10 legs with only 1 or 2 DoF each, and this category of robots
 11 was the topic of our study here. We presented two hexapedal
 12 robots with 6 and 7 motors respectively. The 6 motor BigAnt
 13 has 1-DoF legs; the 7 motor Mechapod has, for all practical
 14 purposes, 2-DoF legs.

15 Under the assumption that we wish, at minimum, to
 16 steer the robots on a horizontal plane, we showed how these
 17 appealing low-complexity morphologies raise unique prob-
 18 lems related to multi-legged locomotion in general, and un-
 19 deractuation in particular. We showed that for the robots in
 20 question, there exist natural ways to produce steering, and il-
 21 luminated some of the special relationship between bilateral
 22 symmetry and steering. We showed that the best steering
 23 gaits we produced do not obey the non-slip contact condi-
 24 tions robot designers usually employ in planning. For the
 25 BigAnt, non-slip conditions would have precluded turning
 26 altogether. For the Mechapod, non-slip gaits do exist, but
 27 under-perform *ad-hoc* steering gaits we tried by a factor of
 28 $\times 4$.

29 The careful examination of mechanism of turning in
 30 both BigAnt and Mechapod lead to some surprising results.
 31 The relationship between Mechapod shape modulation and
 32 steering outcome proved difficult to elucidate. More inter-
 33 estingly, BigAnt motions proved to be independent of speed
 34 and friction coefficient, suggesting that a geometric theory
 35 similar to that which governs slithering snake robots [Gong
 36 et al., 2016] might be applicable. An initial foray into how
 37 the viscous-friction-like relationships of geometric mechan-
 38 ics arise from simple Coulomb friction models can be found
 39 in our recent publication Wu et al. [2019].

40 Taken together this evidence suggests that design of
 41 multi-legged robot gaits raises some new issues related to
 42 phase, but effective solutions for steering are not hard to find,
 43 and do not require the full complexity of 3 or more DoF per
 44 leg. The key issue is that steering gaits, and by extension,
 45 other high-performance maneuvers, must assume that slip-
 46 ping will invariably take place, and be an integral part of the
 47 planned motion. This does not, however, imply that multi-
 48 legged maneuvers require knowledge of friction coefficients
 49 or planning in the full phase space, as some might have as-
 50 sumed. At least for our robots, it seems that some kind of
 51 geometric mechanics theory is lurking just around the cor-
 52 ner, and with it we will be able to reap the benefits of simple
 53 and robust multi-legged robot morphologies.

5 Future work

54 One obvious important direction of future investigation
 55 is developing and validating physics codes for multi-legged

5 locomotion which can handle the persistent slipping that we
 6 have discovered to be necessary for effectively steering our
 7 robots. Besides building better models that include slip-
 8 ping, another interesting approach is to explore the potential
 9 of non-slip gaits with low-DoF legs. We have shown that
 10 Mechapod can have non-slip steering gaits with only 7 mo-
 11 tors; perhaps other low DoF per leg designs can be produced
 12 which have better steering performance. Yet another impor-
 13 tant direction to explore is the high-speed limit: how do the
 14 approaches we studied here extend as robots move faster, in-
 15 eria plays a larger role, and power rather than torque limits
 16 the motors?

Acknowledgements

13 Work on this project was funded by ARO W911NF-14-
 14 1-0573, W911NF-17-1-0243, and W911NF-17-1-0306, as
 15 well as NSF CMMI 1825918.

References

- 17 Anthony M Bloch, Jerrold E Marsden, and Dmitry V
 18 Zenkov. Nonholonomic dynamics. *Not. AMS*, 52(3):320–
 19 329, 2005.
- 20 Xingji Duan, Weihai Chen, Shouqian Yu, and Jingmeng Liu.
 21 Tripod gaits planning and kinematics analysis of a hexa-
 22 pod robot. In *2009 IEEE International Conference on
 23 Control and Automation*, pages 1850–1855. IEEE, 2009.
- 24 I Fitzner, Y Sun, V Sachdeva, and S Revzen. Rapidly proto-
 25 typing robots: Using plates and reinforced flexures. *IEEE
 26 Robotics Automation Magazine*, 24(1):41–47, 3 2017.
 27 ISSN 1070-9932. doi: 10.1109/MRA.2016.2639058.
- 28 Robert Franklin, William J Bell, and Rudolf Jander. Rotational
 29 locomotion by the cockroach *blattella germanica*.
 30 *Journal of Insect Physiology*, 27(4):249–255, 1981.
- 31 Kevin C Galloway, Galen Clark Haynes, B Deniz Il-
 32 han, Aaron M Johnson, Ryan Knopf, Goran A Lynch,
 33 Benjamin N Plotnick, Mackenzie White, and Daniel E
 34 Koditschek. X-rhex: A highly mobile hexapedal robot for
 35 sensorimotor tasks. 2010.
- 36 C Gong, M J Travers, H C Astley, L Li, J R Mendel-
 37 son, D I Goldman, and H Choset. Kinematic gait syn-
 38 thesis for snake robots. *The International Journal of
 39 Robotics Research*, 35(1-3):100–113, 2016. doi: 10.1177/
 40 0278364915593793.
- 41 Duncan W Haldane and Ronald S Fearing. Roll oscilla-
 42 tion modulated turning in dynamic millirobots. In *2014
 43 IEEE International Conference on Robotics and Automa-
 44 tion (ICRA)*, pages 4569–4575. IEEE, 2014.
- 45 Ross L Hatton and Howie Choset. Geometric motion plan-
 46 ning: The local connection, stokes theorem, and the im-
 47 portance of coordinate choice. *The International Journal
 48 of Robotics Research*, 30(8):988–1014, 2011.
- 49 Devin L Jindrich and ROBERT J Full. Many-legged maneu-
 50 verability: dynamics of turning in hexapods. *Journal of
 51 experimental biology*, 202(12):1603–1623, 1999.
- 52 Aaron M Johnson. Robot parkour: the ground reaction com-
 53 plex & dynamic transitions. 2013.
- 54

- 1 Sangbae Kim, Jonathan E Clark, and Mark R Cutkosky.
2 isprawl: Design and tuning for high-speed autonomous
3 open-loop running. *The International Journal of Robotics*
4 *Research*, 25(9):903–912, 2006.
- 5 M Kvalheim, B Bittner, and Revzen S. Gait modeling and
6 optimization for the perturbed stokes regime. *Nonlinear*
7 *Dynamics*, 2019. doi: 10.1007/s11071-019-05121-3.
- 8 Jerry E Marsden and Jim Ostrowski. Symmetries in motion: Geometric foundations of motion control. 1998.
- 9 A J McClung. *Techniques for dynamic maneuvering of hexapedal legged robots*. phdthesis, Stanford University, December 2006.
- 10 D Miller, I Fitzner, SB Fuller, and S Revzen. Focused modularity: Rapid iteration of design and fabrication of a meter-scale hexapedal robot. In *Assistive Robotics: Proceedings of the 18th International Conference on CLAWAR 2015*, pages 430–438. World Scientific, 2015. doi: 10.1142/9789814725248_0053.
- 11 J Proctor and P Holmes. Steering by transient destabilization in piecewise-holonomic models of legged locomotion. *Regular and Chaotic Dynamics*, 13(4):267–282, 2008.
- 12 Andrew O Pullin, Nicholas J Kohut, David Zarrouk, and Ronald S Fearing. Dynamic turning of 13 cm robot comparing tail and differential drive. In *2012 IEEE International Conference on Robotics and Automation*, pages 5086–5093. IEEE, 2012.
- 13 S Revzen, D E Koditschek, and R J Full. *Progress in motor control - a multidisciplinary perspective*, chapter Towards testable neuromechanical control architectures for running, pages 25–56. Springer Science+Business Media, LLC - NY, 2008. doi: 10.1007/978-0-387-77064-2_5F3.
- 14 Shibendu Shekhar Roy and Dilip Kumar Pratihar. Kinematics, dynamics and power consumption analyses for turning motion of a six-legged robot. *Journal of Intelligent & Robotic Systems*, 74(3-4):663–688, 2014.
- 15 Vikram Sachdeva, Dan Zhao, and Shai Revzen. Cockroaches always slip a lot. In *The Society for Integrative and Comparative Biology Annual Meeting*, 2018.
- 16 Uluc Saranli, Martin Buehler, and Daniel E Koditschek. Rhex: A simple and highly mobile hexapod robot. *The International Journal of Robotics Research*, 20(7):616–631, 2001.
- 17 J Sastra, S Revzen, and M Yim. Softer legs allow a modular hexapod to run faster. In *Climbing and Walking Robotics (CLAWAR)*, 2012. doi: 10.1142/9789814415958_0065.
- 18 Jimmy Sastra, WG Bernal-Heredia, Jonathan Clark, and Mark Yim. A biologically-inspired dynamic legged locomotion with a modular reconfigurable robot. In *Proc. of DSCE ASME Dynamic Systems and Control Conference*, 2008.
- 19 John Schmitt and Philip Holmes. Mechanical models for insect locomotion: dynamics and stability in the horizontal plane i. theory. *Biological cybernetics*, 83(6):501–515, 2000.
- 20 Justin E Seipel, Philip J Holmes, and Robert J Full. Dynam-
ics and stability of insect locomotion: a hexapedal model for horizontal plane motions. *Biological cybernetics*, 91(2):76–90, 2004.
- 21 Simon Wilshin, Michelle A Reeve, G Clark Haynes, Shai Revzen, Daniel E Koditschek, and Andrew J Spence. Longitudinal quasi-static stability predicts changes in dog gait on rough terrain. *Journal of Experimental Biology*, 220(10):1864–1874, 2017.
- 22 Ziyou Wu, Dan Zhao, and Shai Revzen. Coulomb friction crawling model yields linear force–velocity profile. *Journal of Applied Mechanics*, 86(5):054501, 2019.
- 23 David Zarrouk and Ronald S Fearing. Controlled in-plane locomotion of a hexapod using a single actuator. *IEEE Transactions on Robotics*, 31(1):157–167, 2015.
- 24 David Zarrouk, Duncan W Haldane, and Ronald S Fearing. Dynamic legged locomotion for palm-size robots. In *Micro-and Nanotechnology Sensors, Systems, and Applications VII*, volume 9467, page 94671S. International Society for Optics and Photonics, 2015.
- 25 D Zhao and S Revzen. Slipping helps steering in a multi-legged robot. In *Dynamic Walking*, 2016.
- 26 D Zhao, C M Schaffer, and Revzen S. Steering hexapedal robots. In *Workshop on Miniature Legged Robots, Conference on Robotics Science and Systems*, 2015.
- 27 V Zolotov, L Frantsevich, and EM Falk. The kinematics of phototactic turns in the honeybee. *J. comp. Physiol.*, 97:339–353, 1975.

Appendix A: Pitch and Roll data

Here we provide some examples (world frame z motion of COM Fig. 21; pitch and roll angle Fig. 21) of BigAnt, demonstrating its stability .

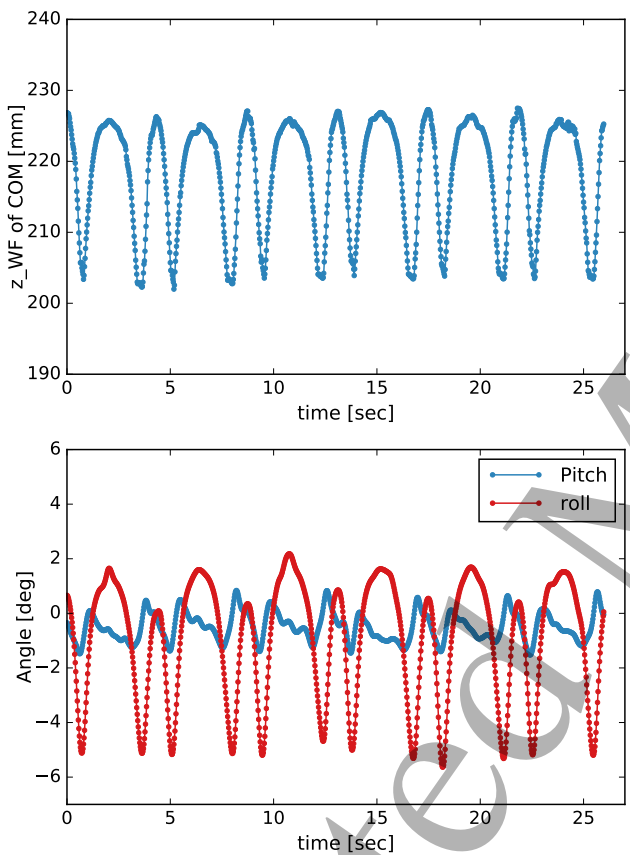


Fig. 21: World frame z motion of BigAnt COM (top), pitch and roll (bottom) with $s = 0.75$ $f = 0.22\text{Hz}$